General Disclaimer

One or more of the Following Statements may affect this Document

- This document has been reproduced from the best copy furnished by the organizational source. It is being released in the interest of making available as much information as possible.

- This document may contain data, which exceeds the sheet parameters. It was furnished in this condition by the organizational source and is the best copy available.

- This document may contain tone-on-tone or color graphs, charts and/or pictures, which have been reproduced in black and white.

- This document is paginated as submitted by the original source.

- Portions of this document are not fully legible due to the historical nature of some of the material. However, it is the best reproduction available from the original submission.

NASA Technical Memorandum 73298

Baseline Monitoring Using Aircraft Laser Ranging

W. B. Krabill
F. E. Hoge
and
C. F. Martin

June 1982

National Aeronautics and Space Administration
Goddard Space Flight Center
Wallops Flight Center
Wallops Island, Virginia 23337

NASA Technical Memorandum 73298

Baseline Monitoring Using Aircraft Laser Ranging

W. B. Krabill and F. E. Hoge

NASA Goddard Space Flight Center
Wallops Flight Center
Wallops Island, Virginia 23337

and

C. F. Martin

EG&G Washington Analytical Services Center
Riverdale, Maryland 20840

National Aeronautics and
Space Administration

Goddard Space Flight Center
Wallops Flight Center
Wallops Island, Virginia 23337

BASELINE MONITORING USING AIRCRAFT LASER RANGING

W. B. Krabill
F. E. Hoge
NASA Wallops Flight Center
Wallops Island, VA 23337

and

C. F. Martin
EG&G Washington Analytical Services Center, Inc.
Riverdale, MD 20840

INTRODUCTION

Current interests in the modeling of geodynamics phenomena include crustal movements over a wide range of distances. At the long end, measurements are desired between tectonic plates over intercontinental distances of up to about 10,000 km. On the other end of the range scale, measurements are desired within a few hundred kilometers of those fault boundaries at which earthquakes are considered most likely to occur. For the latter scale of monitoring, proposals have been made for space techniques bearing the acronyms CLOGEOS (Mueller, et al., 1975; Smithsonian Astrophysical Observatory, 1977), SPEAR (Vonbun et al., 1977), SGRS (Smith and Tapley, 1979), and simply Spaceborne Ranging System (Smith, 1978; Kahn, et al., 1979). The basic concept includes a laser system capable of accurate pointing carried on either a space shuttle or a free flying spacecraft, and making ranging measurements to ground based retro-reflectors deployed in some array over an area for which crustal movements are desired to be monitored over a period of years. It is required that the array extend into regions for which no motion is to be expected, since only relative distances between reflectors are monitored. Studies suggest that some eight to ten spaceborne flights over a retro-field are potentially capable of estimating baseline distances up to several hundred kilometers, with accuracies at the 1-2 cm level (Kahn et al., 1979; Pavlis, 1979; Kumar and Mueller, 1978; Smith, 1978). The frequency with which the set of passes would need to be repeated depends, of course, on the expected level of tectonic activity, but repeats at intervals of at least six to twelve months would be required for any relatively active region.

Although the spaceborne laser may be expensive to build, it is presently well within the state-of-the-art to build an instrument with the required 1-2 cm ranging accuracy, and to supply it with a sufficiently accurate pointing system. Assuming the laser ranger to be accurately calibrated, the major error source remaining has been found to be geopotential model errors (Kahn et al., 1979). The continued development of new gravity models suggests that the geopotential problem may not be severe for a spaceborne laser launch in the mid to late 1980's. However, it is not presently clear whether the meteorological problems can be solved without the utilization of a two color laser.

Due to the lack of experience with a spaceborne laser tracking a ground network of retro-reflectors, and availability of an airborne scanning laser on the NASA Wallops C-54 aircraft, an experiment was performed at Wallops Flight Center in May 1979 to attempt to identify some of the problems likely to be encountered by a spaceborne laser. Although the dimensions of the retro-reflector array utilized for the aircraft tests were much smaller than those contemplated for tracking from space, the ratio of reflector separation to aircraft altitude was roughly comparable to those frequently proposed for a spacecraft monitoring reflectors separated by 50 km from an altitude of 1000 km. Thus, range measurement sensitivity to baseline errors should be similar for both the aircraft and spaceborne situations. Of course, dynamic modeling of aircraft and spacecraft motions are drastically different, so optimum schemes for tracking the retro-reflectors will also be different.

In addition to its application for studying potential problems associated with spaceborne laser ranging, laser ranging from aircraft is now of some interest in its own right. Reasons for this include:

(1) The aircraft system and operation is potentially less expensive.

(2) An aircraft system could be developed and baseline monitoring initiated prior to the launch of a spaceborne system, thus making available several years of crustal movement data before beginning the long term monitoring by a spaceborne system.

(3) Monitoring of relatively small areas (~ 100 km) is of particular interest (Kaula, 1978) at the current stage in the understanding of crustal motion.

(4) Some simulations have indicated (Kumar, 1976; Kumar and Mueller, 1978) that aircraft ranging is very valuable in strengthening baseline determinations based on spaceborne laser ranging.

In this paper, we will discuss first the laser system, the types of measurements it is capable of making and the type of experiment planned for the spaceborne laser simulation. Next, we consider some simulation results for baseline estimation using an airborne scanning laser system. Finally, we discuss the results from flight tests and their implications for future spaceborne or aircraft laser tracking.

INSTRUMENTATION AND EXPERIMENT DESCRIPTION

The laser used for the flight tests was the Airborne Oceanographic Lidar (AOL), a conically scanning pulsed laser system designed primarily to perform field demonstration and technology transfer experiments in the areas of airborne bathymetry and laser induced fluorescence. An outline drawing of the AOL installed in the Wallops C-54 aircraft used for the experiment is shown in Figure 1. In both the bathymetry and fluorosensing modes, the instrument operation includes precision ranging and this was the basic measurement used for the retro-reflector tests discussed in this paper. However, operation was in the nominal "bathymetry" mode, so that the backscattered return pulse waveform was recorded for post-flight analysis. The laser was operated at 400 pps, scanning at a 5 Hz rate, thus providing ~80 pulses per scan. The off-nadir scan angle was set at 15°, the maximum available for the AOL. The laser was operated in the UV (337.1 nm) with a nominal beam width of 20 mr, and transmitted pulse width of 9 ns.

Based on these parameters and referring to Figure 2 we see that for any height H, the scan radius (for a circular scan) is H tan α. For 80 pulses per scan, the distance between the center of adjacent illuminated areas is then approximately $2\pi H \tan \alpha/80$ or 0.021 H for a 15° scan angle. On the other hand, for a circular cross-section laser beam pattern of 20 mr angular divergence, the laser terrestrial pulse pattern will be an ellipse with minor diameter equal to $(H/\cos \alpha)(0.020) \approx 0.021H$. Thus, the footprint pattern for an individual scan can be closely approximated by a set of 80 touching circles around the scan, as shown in Figure 3, independent of aircraft altitude. The actual AOL footprint pattern is somewhat more complex (AVCO, 1975), but the above qualitative conclusion is still valid.

Next, we consider the aircraft motion between scans. We would also like to have the footprints from adjacent scans to at least touch. Thus, if we set the distance moved between scans equal to footprint diameter, we obtain

$$V/5.06 \text{ scans/sec} < 0.021H,$$

with V the aircraft speed. Substituting a nominal speed of 76 m/sec for the Wallops C-54 aircraft, we obtain

$$H > 715 \text{ m}.$$

For this altitude, the dimensions of the retro-reflector field then depend upon the number of rows which it is desired to cover. However, because of the difficulty in navigating an aircraft exactly down the middle of the array, it is desirable to have rows

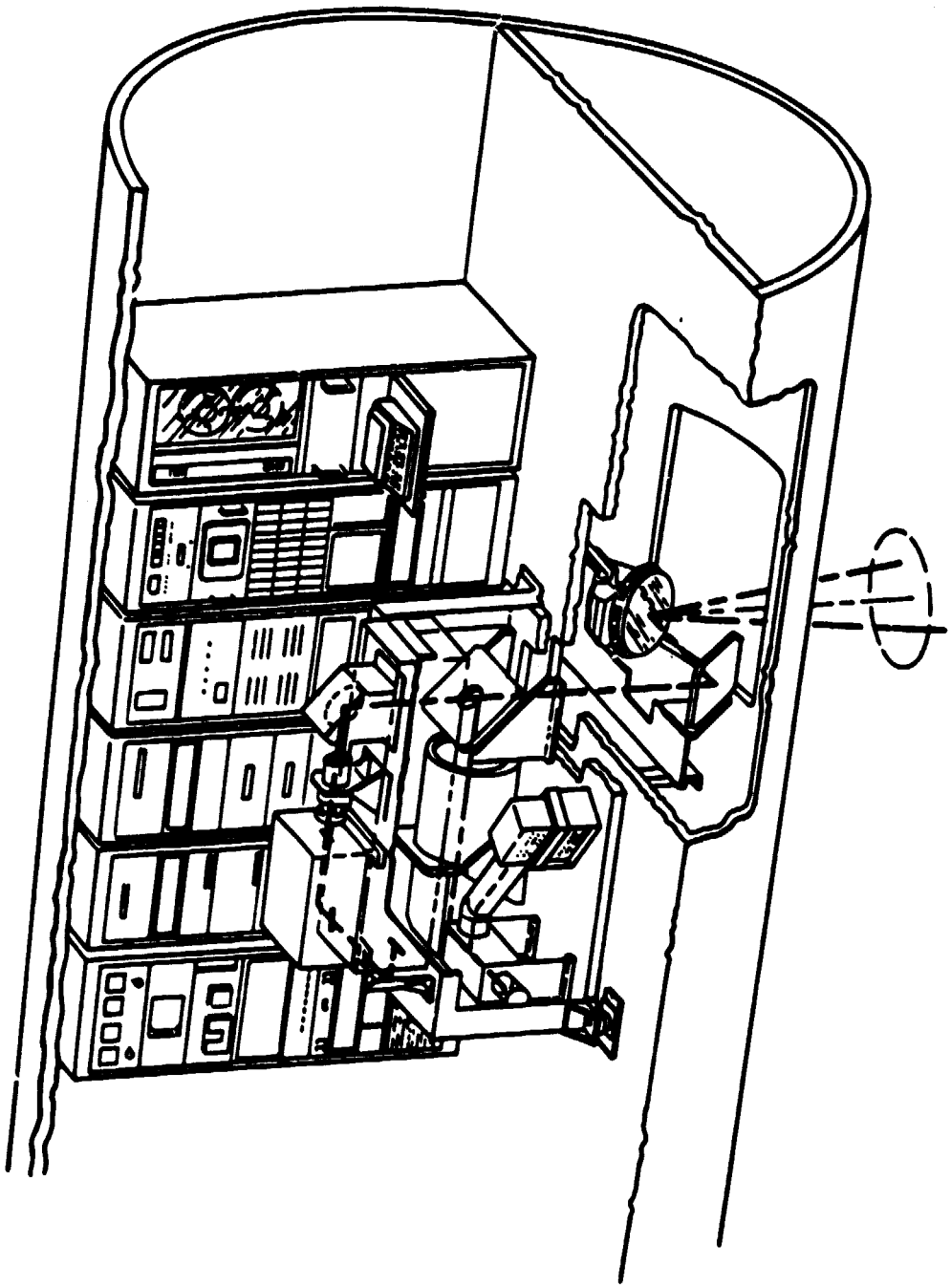

Figure 1. Installation arrangement of the AOL on the NASA C-54 aircraft.

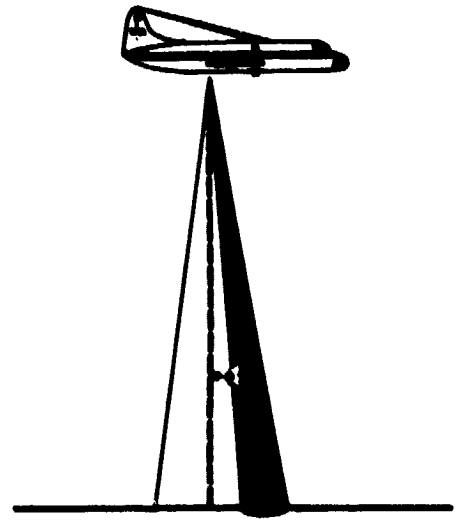

Figure 2. AOL scan geometry.

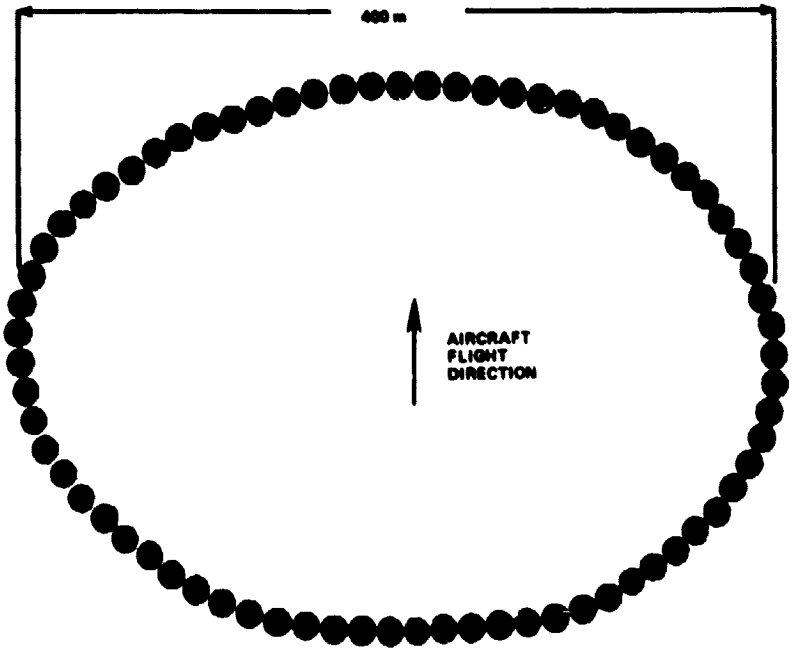

Figure 3. Laser footprints for an AOL scan from 750 m altitude showing near total coverage of 400 m swath along flight path. Off nadir angle of 15° and beam divergence of 20 mr assumed. Relative footprint spacing is independent of altitude.

positioned slightly within the nominal scan pattern. The scan pattern has a diameter of 2H tan α, or 383 m for the 715 m altitude. If a flight pass is to cover the entire retro field, then we are led to a retro field width of 300-350 m, allowing for expected aircraft errors in following a planned flight pass. Figure 4 shows a retro field based on these dimensions which was used as a base field for performing error analyses.

ESTIMATION ALGORITHM

In some schemes which have been proposed and investigated for baseline estimation using laser ranging from aircraft (Kumar, 1976; Kumar and Mueller, 1978), multiple ranges (> 4) are considered to be made at each time point at which data is taken. Aircraft position can thus be estimated simultaneously with the reflector positions and no aircraft dynamics are necessary. In practice, particularly with centimeter level results desired, simultaneous ranging to multiple reflectors cannot be achieved. Simultaneously transmitted pulses will not be received simultaneously and aircraft motion between pulse return times can approach the centimeter level for an aircraft flying at 10,000 m. For the scanning AOL flying along an array of three rows of retros such as is shown in Figure 3, there will be a maximum of four hits within one scan. Thus, for the C-54, there will be a maximum of four reflector hits for an aircraft movement of 15 m, and some modeling of aircraft motion during this time is required.

The model adopted is basically that which has been implemented in the KAPPA program (Aldrich, 1970) which is presently used for estimating aircraft and rocket trajectories from radar tracking data at NASA Wallops Flight Center. The state and measurement models are taken to be

$$X_n = \Phi_n X_{n-1} + q_n \tag{1}$$

$$m_n = A_n X_n + B_n k + \epsilon_n \tag{2}$$

where

X_n is the aircraft state at time t_n

Φ_n is the state transition matrix transforming the state from time t_{n-1} to time t_n

q_n is the "state" noise at time t_n

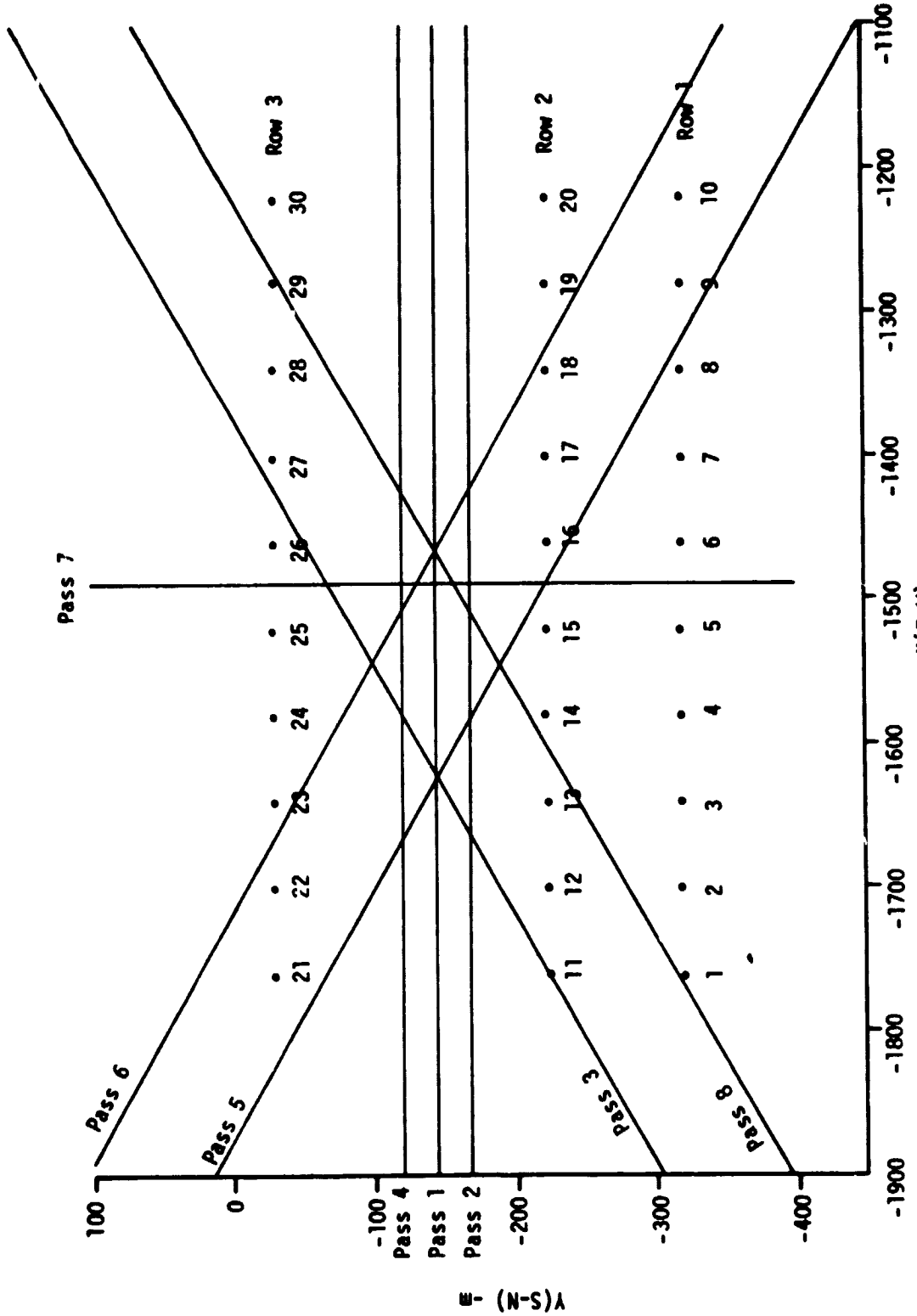

Figure 4. Reflector geometry and aircraft tracks used for simulations.

m_n is the measurement (residual) at time t_n

$A_n = \frac{\partial m_n}{\partial X_n}$ is the partial of the measurement at time t_n with respect to the aircraft state at time t_n

k is the vector of station position states which are to be estimated whenever all data is available

$B_n = \frac{\partial m_n}{\partial k}$ is the partial of the measurement at time t_n with respect to the station position set

ϵ_n is the measurement noise at time t_n .

To complete the model, we make the assumptions that the state and measurement noise are zero mean and uncorrelated in time or with each other:

$$E(q_n) = E(\epsilon_n) = 0 \tag{3}$$

$$E(q_n q_n^T) = Q_n \tag{4}$$

$$E(q_n q_m^T) = E(\epsilon_n \epsilon_m^T) = 0, \; m \neq n \tag{5}$$

$$E(q_n \epsilon_m^T) = 0 \tag{6}$$

$$E(\epsilon_n \epsilon_n^T) = W_n^{-1} \tag{7}$$

The total state includes the aircraft position and velocity and the coordinates of the retro-reflectors, with non-zero state noise considered only for aircraft position and velocity. Due to the high measurement frequency, and the assumption of aircraft flight paths with low dynamics (i.e., near straight line), the state transition model includes only constant velocity motion between measurements. Radar tracking of the aircraft (range, azimuth, and elevation) and laser ranging to the retro-reflectors constitute the measurement set. In addition, each aircraft pass has a starting vector with associated state covariance. In general, a priori information will be used for each retro-reflector, with the objective being to at least constrain the orientation of the retro array.

The desired solution for the station coordinates k is the one with minimum variance, allowing for the uncertainties in the aircraft trajectory model and the measurement

errors. A Kalman filter solution for the above equations could be developed, with incremental adjustments to the station coordinates made with the addition of each new measurement. However, since only small adjustments to station coordinates are expected in geodynamic applications, we consider an implementation of an equivalent minimum variance estimation in which the solution is partitioned as suygested by Equation (2) into aircraft states and station position states. In this procedure the aircraft state is sequentially estimated with fixed reflector positions, but the normal equations are simultaneously accumulated so that adjustments can later be computed, based on the combined measurements from any number of passes. Except for the inclusion of aircraft dynamics, this is the same partitioning procedure one would expect to use for multiple (> 4) simultaneous aircraft range measurements to retro-reflectors. If there are a total of M aircraft passes, the combined adjustment for the station positions is

$$k = \left[\sum_{n=1}^{M} \Lambda_n + V_{ko}^{-1} \right]^{-1} \sum_{n=1}^{M} h_n \tag{8}$$

where V_{ko} is the variance covariance matrix of the a priori coordinates. Assuming there to be N measurements for the n'th pass, Λ_n and h_n are defined by

$$\Lambda_n = \sum_{i=1}^{N} \left(B_i^T W_i B_i - \left\{ A_i^T W_i B_i \right\}^T \right.$$
$$\left. \times \left(V_i^{-1} + \Phi_{i+1}^T Q_{i+1}^{-1} \Phi_{i+1} \right)^{-1} \left\{ A_i^T W_i B_i \right\} \right) \tag{9}$$

$$h_n = \sum_{i=1}^{N} \left(B_i^T W_i m_i - \left\{ A_i^T W_i B_i \right\}^T \left(V_i^{-1} + \Phi_{i+1} Q_{i+1}^{-1} \Phi_{i+1} \right)^{-1} \right.$$
$$\left. \times \left\{ A_i^T W_i m_i \right\} \right) \tag{10}$$

with the quantities in braces defined by the recursion relations

$$\left\{ A_i^T W_i B_i \right\} = A_i^T W_i B_i + \left(Q_i + \Phi_i V_{i-1} \Phi_i^T \right)^{-1}$$

$$x \; \Phi_i V_{i-1} \left\{ A_{i-1}^T W_{i-1} B_i \right\} \tag{11}$$

$$\left\{ A_i^T W_i m_i \right\} = A_i^T W_i m_i + \left(Q_i + \Phi_i V_{i-1} \Phi_i^T \right)^{-1}$$

$$x \; \Phi_i V_{i-1} \left\{ A_{i-1}^T W_{i-1} m_{i-1} \right\} \tag{12}$$

These recursion relations are initialized by

$$\left\{ A_o^T W_o B_o \right\} = 0 \tag{13}$$

$$\left\{ A_o^T W_o m_o \right\} = 0 \tag{14}$$

V_i is also obtained via a recursion relation

$$V_i^{-1} = A_i^T W_i A_i + \left(\Phi_i V_{i-1} \Phi_i^T + Q_i \right)^{-1} \tag{15}$$

with V_o the a priori covariance matrix of the aircraft state. Since the N + 1 state for a pass is not defined, we must have

$$\left[V_N^{-1} + \Phi_{N+1}^T Q_{N+1}^{-1} \Phi_{N+1} \right]^{-1} = V_N \tag{16}$$

Finally, for computations in which Q_i^{-1} does not always exist, we make the substitution

$$\left[V_i^{-1} + \phi_{i+1}^T Q_{i+1}^{-1} \phi_{i+1} \right]^{-1}$$

$$\longrightarrow \phi_{i+1}^{-1} Q_{i+1} \left[V_i^{-1} \phi_{i+1}^{-1} Q_{i+1} + \phi_{i+1}^T \right]^{-1} \qquad (17)$$

The inverse of the state transition matrix ϕ_i always exists.

SIMULATION RESULTS

Groundtracks for eight passes across a field of 30 retro-reflectors are shown in Figure 4, along with the reflector locations. Several different altitudes are assumed, as indicated in Table I which also shows the number of reflector hits for each pass. All passes parallel to the rows of reflectors were at an altitude of 750 m, allowing the footprint pattern to intersect all rows even with the aircraft considerably off the center of the array field. The passes across the rows were all at higher altitudes in order to increase the probability of obtaining hits from all three rows on a single scan.

Since the planned tests at Wallops included radar tracking of the aircraft, the simulated data included radar range, azimuth, and elevation information with accuracies approximately equivalent to observed noise levels at a 10 pps data rate. To reduce computer time requirements for the simulations, the radar data rate was decreased by a factor of five, with noise levels reduced by $\sqrt{5}$. Table II summarizes the data and accuracies simulated.

In addition to being a function of the assumed data and its accuracy, the simulated reflector position accuracies are also dependent on the aircraft state noise. For the simulations performed, the assumed state noise covariance was

$$Q_n = \phi_n \begin{bmatrix} 0 & 0 & 0 & 0 & 0 & 0 \\ 0 & 0 & 0 & 0 & 0 & 0 \\ 0 & 0 & 0 & 0 & 0 & 0 \\ 0 & 0 & 0 & V_{qx}^2 & 0 & 0 \\ 0 & 0 & 0 & 0 & V_{qy}^2 & 0 \\ 0 & 0 & 0 & 0 & 0 & V_{qz}^2 \end{bmatrix} \phi_n^T$$

TABLE I. SIMULATED REFLECTOR HITS BY AIRCRAFT LASER

Row No.	Refl. No.	Number of Hits: Pass 1 H=750m Az=0°	Pass 2 H=750m Az=0°	Pass 3 H=950m Az=30°	Pass 4 H=750m Az=0°	Pass 5 H=950m Az=-30°	Pass 6 H=850m Az=-30°	Pass 7 H=1050m Az=-90°	Pass 8 H=950m Az=30°	Total
1	1	4	4	1	6	5	0	12	1	33
1	2	3	4	2	6	2	0	4	2	23
1	3	5	2	2	5	4	11	2	2	33
1	4	3	3	4	5	2	5	4	2	28
1	5	4	3	4	5	4	3	3	3	29
1	6	4	4	5	6	2	3	2	4	30
1	7	4	4	0	6	2	3	3	4	26
1	8	5	2	0	4	2	1	3	5	22
1	9	4	3	0	5	2	3	4	8	29
1	10	4	3	0	5	2	2	12	0	28
2	11	2	1	1	2	4	4	12	3	29
2	12	2	2	3	3	3	4	4	4	25
2	13	3	1	2	2	2	3	4	3	20
2	14	3	1	3	3	3	2	2	4	21
2	15	2	2	2	3	2	3	3	2	19
2	16	2	2	2	1	3	3	2	2	17
2	17	2	2	3	3	2	2	3	2	19
2	18	3	2	4	2	2	2	4	3	22
2	19	2	1	10	3	2	3	5	3	29
2	20	2	2	0	3	2	3	12	4	28
3	21	2	5	3	2	1	2	12	9	36
3	22	3	3	2	3	2	2	3	5	23
3	23	2	3	4	2	3	2	4	3	23
3	24	2	2	4	2	3	3	2	3	21
3	25	3	3	2	2	2	2	2	2	18
3	26	2	4	2	2	5	3	2	2	22
3	27	3	3	2	3	3	2	2	3	21
3	28	2	2	1	2	12	2	3	2	26
3	29	2	3	2	2	0	3	5	2	19
3	30	3	4	4	3	0	5	16	4	39
Total		87	80	74	101	83	86	151	96	758

TABLE II. DATA ACCURACIES ASSUMED FOR SIMULATIONS OF REFLECTOR POSITION ESTIMATIONS

DATA TYPE	NOISE LEVEL	DATA RATE
Laser	10 cm	Whenever reflector within footprint of 400/sec pulse rate
Radar - Range	.45 m	2/sec
Radar - Azimuth	.22 mils	
Radar - Elevation	.22 mils	

with $V_{qx} = V_{qy} = V_{qz} = 1$ m/sec. This choice has the effect, as it must for the scanning mode of reflector tracking, of providing some dynamic constraints between laser measurements while allowing for the inability to adequately model the aircraft motion for a complete pass across the reflector field. As in all such applications of a sequential filter, however, the choice of numerical values for Q_n is largely empirical, and the above choice made may not be completely optimal.

Figures 5-7 summarize some of the simulation results for baseline accuracy, with the four corner reflectors constrained with standard deviation (one sigma) of 1 cm in each coordinate. Figure 5 shows the sigmas for the baselines relative to one of the constrained reflectors, and the sigmas for baselines relative to the other constrained reflectors are similar in magnitude and behavior. The sigmas lie generally within a band between 20 and 30 cm and, in some cases, slightly decrease with increasing baseline distance. The anomalous behavior at the shorter baseline is reasonable on the basis of the scanning geometry and the associated characteristic of adjacent (in time) hits of reflectors on the same row.

Figure 6 shows baseline sigmas between unconstrained reflectors with most of the numbers between 30 and 40 cm. The baselines between the first and third rows are less well determined than those between the other rows for a given baseline distance, for reasons that are not immediately obvious. However, the middle row of reflectors is, in general, better determined than the outer two rows, as will be more clearly demonstrated by the height accuracies discussed below.

Figure 7 shows the baseline sigmas for the total set of baselines within the second row, no reflectors of which are constrained. Here, the sigmas are around 30 cm, and the lowest sigmas are for the shorter baselines. This characteristic must be due to the use of relatively low aircraft state noise, since a high percentage of the passes are along the rows and only dynamics can provide strength between adjacent reflectors within a row.

Finally, Figure 8 shows the sigmas for the reflector heights relative to the plane determined by constrained reflectors on the corners of the array. The sigmas are 5-6 cm for the row one and row three, and about 4 cm for row two.

It will be noted that the height sigmas are much smaller than the baseline sigmas, which can be attributed to the scan geometry as shown in Figure 2. With the 15° scan angle, the ranging measurements are much more sensitive to height than to horizontal positioning. For example, the laser range from the aircraft to reflector i can be written

$$R = (x_a - x_i)^2 + (y_a - y_i)^2 + (z_a - z_i)^2$$

where (x_a, y_a, z_a) are the aircraft coordinates and (x_i, y_i, z_i) are the reflector coordinates. Then

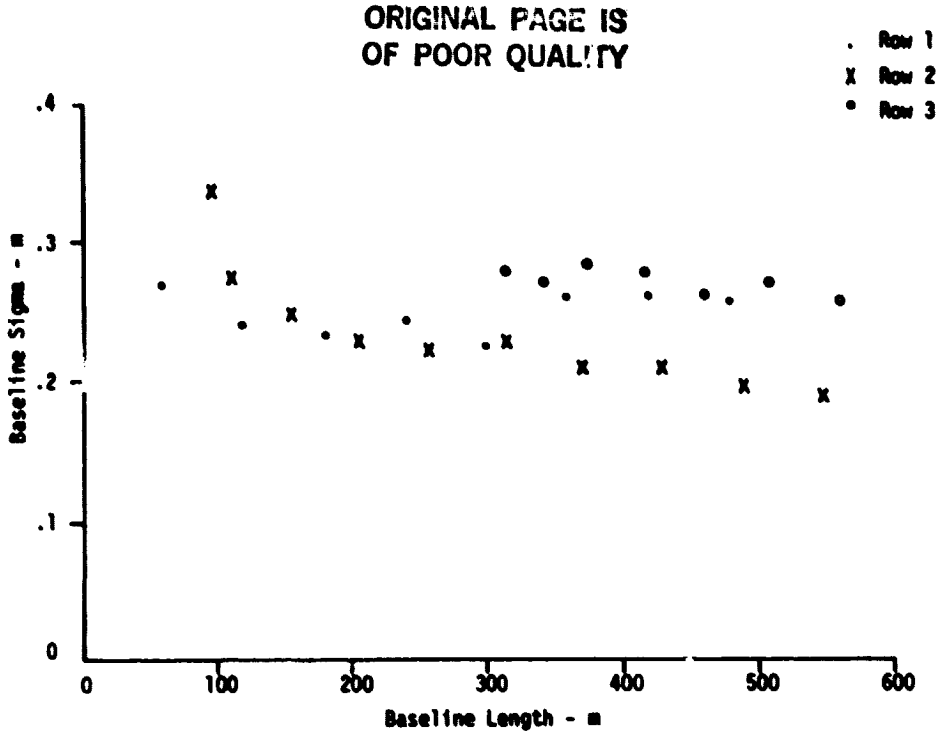

Figure 5. Sigmas for baselines relative to constrained reflector no. 1.

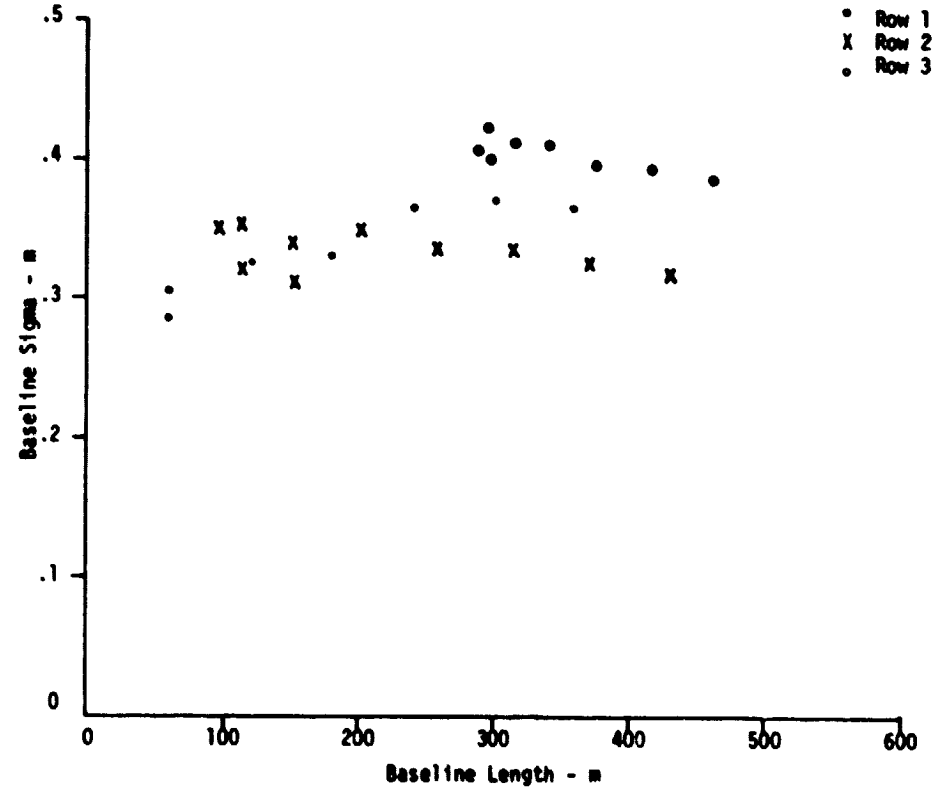

Figure 6. Sigmas for unconstrained reflectors relative to reflector no. 3.

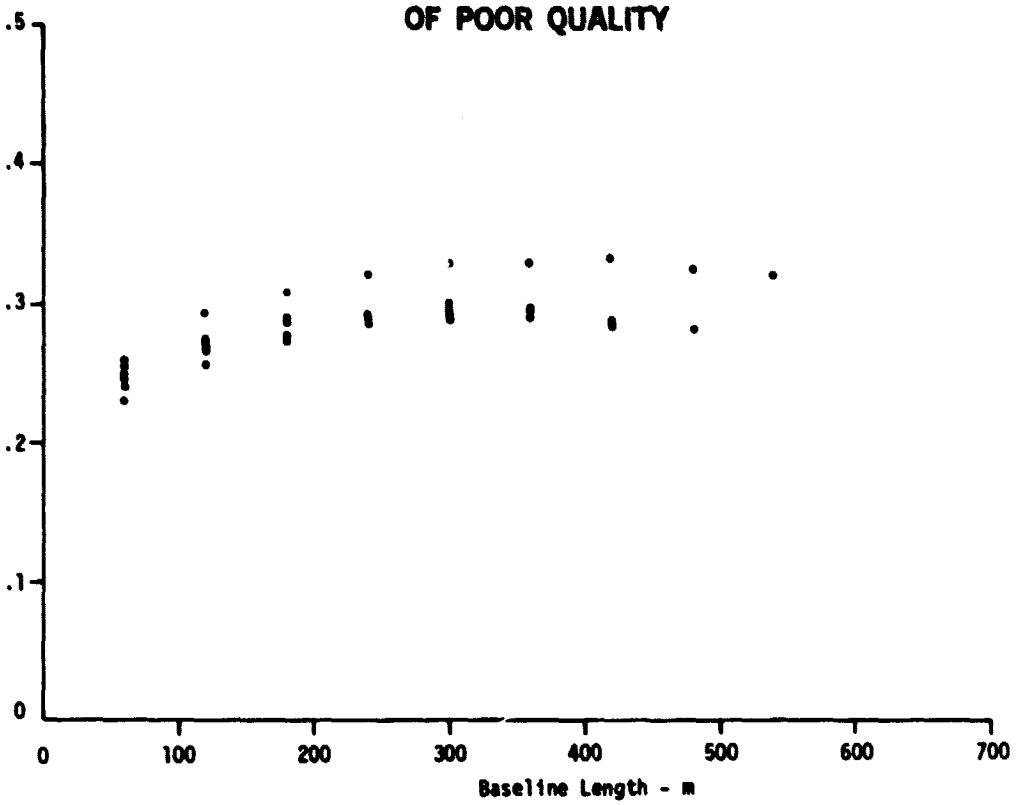

Figure 7. Sigmas for baselines in row no. 2.

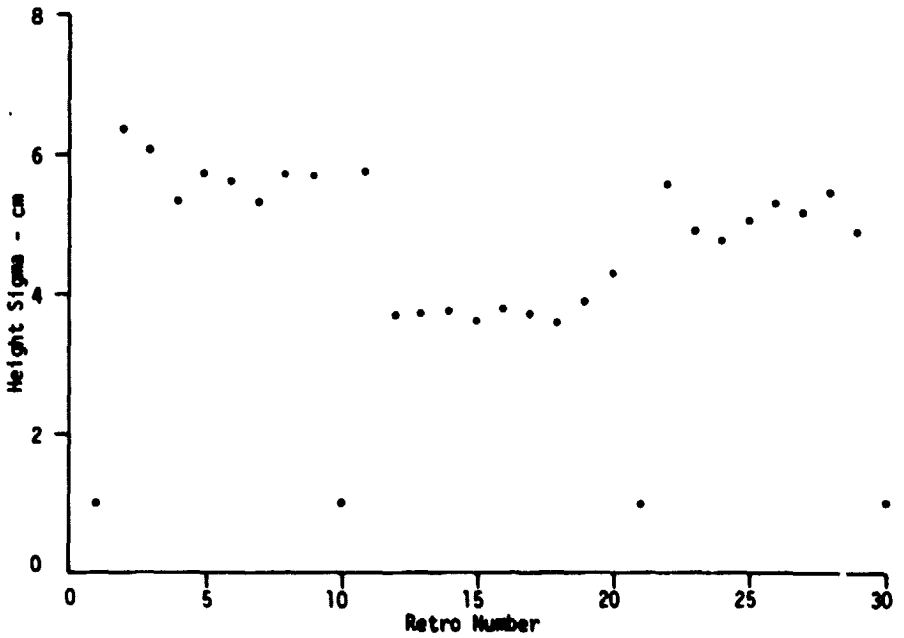

Figure 8. Height sigmas, with retros 1, 10, 21, 30 constrained via a priori sigmas of 1 cm.

$$\frac{\partial R}{\partial x_i} = -(x_a - x_i)/R$$

$$\frac{\partial R}{\partial y_i} = -(y_a - y_i)/R$$

$$\frac{\partial R}{\partial z_i} = -(z_a - z_i)/R$$

For simplicity choosing a point for which $y_a = y_i$, then from Figure 2,

$$\frac{\partial R}{\partial x_i} = -\sin\phi$$

$$\frac{\partial R}{\partial z_i} = -\cos\phi$$

The ratio of these sensitivities is then

$$\frac{\partial R}{\partial z_i} \Big/ \frac{\partial R}{\partial x_i} = \cot\phi$$

For $\phi = 15°$, this ratio is 3.7. From Figure 5, we find an average sigma for baselines relative to a constrained reflector of about 25 cm, and from Figure 8 we have an average height sigma of about 5 cm. The height sigma is thus greater than the baseline sigma by about a factor of five, in order of magnitude quite close to 3.7. It follows from the above range partials that equivalent height and baseline sigmas would be expected for an off-nadir scan angle of 45°. For the same number of measurements given in Table I and the same measurement accuracy given in Table II, the sigmas in Figures 5-7 would be reduced by a factor of sin 45°/sin 15° = 1.4. It should also be noted, however, that with the 45° scan angle, the aircraft altitude should be reduced by a factor of tan 45°/ tan 15° = 3.7. Alternatively, the dimensions for the array field, and the abscissa scale in Figures 5-7 could be increased by the same factor.

EXPERIMENTAL RESULTS

A series of flights over a retro-reflector field, similar to that described above, was performed at Wallops Flight Center, Wallops Island, Virginia, on May 1, 1979. Reflectors were deployed in three rows along one of the Wallops aircraft runways, as shown in Figure 9. The area and retro configuration were chosen because of the existence of a number of surveyed markers along the runway, and the convenience of the area for missions utilizing Wallops Flight Center aircraft.

The retro array shown in Figure 9 was optimum for an aircraft pass at approximately 750 m altitude, based on the scan pattern discussion above and the desire for the scan pattern diameter to slightly exceed the width of the array. Flights were also flown at several higher altitudes in order to determine the variations with altitude of ground return signals as well as return signals from the retros. Two types of reflectors were included: (1) open-faced 25 mm nominal diameter reflectors with 1 mr beam divergence, elevated approximately 1 m above ground level, and (2) solid quartz 50 mm diameter retro reflectors with 0.1 mr beam divergence. The latter reflectors were at ground level.

Each pass of the aircraft across the retro field was tracked by an FPS-16 C-Band radar located near the runway along which the retros were deployed. The aircraft trajectory determined from this radar tracking, along with the AOL scan azimuth and aircraft orientation (pitch, roll, heading as measured by the aircraft LTN-51 Inertial Navigation System), were sufficient to position the laser footprint with an accuracy of 10-20 m. Return pulses of large amplitude and having a footprint center within 20 m of a retro were thus readily identifiable as being due to, or at least including, a retro return. For the elevated reflectors, confirmation of retro hits is also possible on the basis of the shorter measured ranges.

Table III summarizes the total number of identified retro hits across the 32 reflector array, with typically 6-10 hits per pass. This is a much smaller number than that obtained in the simulations summarized in Table I, and has been attributed to a highly elliptical laser cross-sectional beam pattern. The measured N_2 laser beam pattern has an eccentricity of approximately 0.9, with the major axis of the ellipse rotated ~15° counter clockwise from the aircraft wing axis. Simulations accounting for the elliptical beam pattern have confirmed that the number of hits obtained is consistent with the reflectors expected to be included in footprints.

Although the two types of retros used differ substantially in area, return beam divergence and cost, there were no discernible differences in the return pulse amplitude or shape that could be reasonably attributed to retro type. There were, however, significant variations in return pulse amplitude that could be attributed to the retro being in the center of the laser beam.

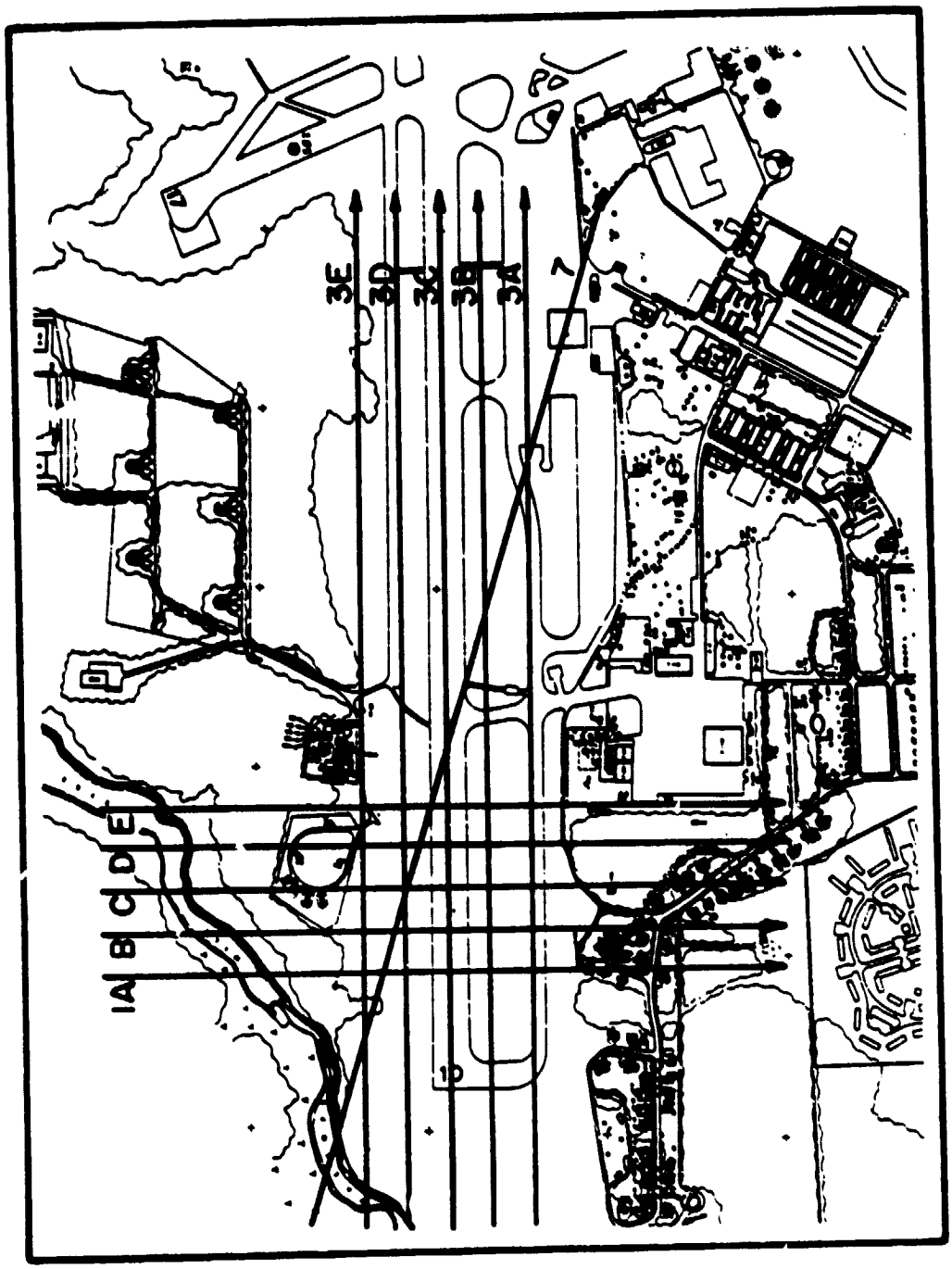

Figure 9. Aircraft flight lines along Wallops runway for retro-reflector tests.

TABLE III. NUMBER OF GROUND REFLECTOR HITS BY AIRCRAFT BORNE LASER ON MAY 1, 1979 MISSION AT NASA WALLOPS FLIGHT CENTER.

Pass No.	Altitude	Plane Direction	Total No. of Hits	No. of Double Hits	No. of Triple Hits
1C/2	2650'	South to North	15	3	2
1C/3	2650'	South to North	12	-	2
3C/4	2650'	West to East	3	-	-
3C/5	2650'	West to East	14	3	-
3C/6	2650'	West to East	8	1	-
3C/7	3500'	West to East	8	1	-
3C/8	3500'	West to East	1	-	-
3C/9	4500'	West to East	5	1	-
3C/10	4500'	West to East	3	-	-
3C/11	4500'	West to East	2	-	-
7/1	4500'	NW to SE	2	-	-
7/2	4500'	NW to SE	5	-	-

Figure 10 shows the aircraft path for one of the passes, and identifies the retros conclusively hit during the pass, based on return pulse amplitude. The figure also shows a location from which a large amplitude return was obtained, but which definitely did not include any of the retros. This problem suggested that the intensity of return pulses be examined in the runway area to determine strongly reflecting regions that could cause difficulties in identifying true reflector hits. The contour in Figure 11, based on the intensities of the 400/sec return pulses from pass 3C/5 on May 1, shows not only the high intensities obtained from the reflectors, but also the high intensities obtained from the concrete portions of the aircraft runway itself. In this figure the sizes of the retro-reflectors appear somewhat enlarged due to the particular technique used for enhancement of the contoured projection.

CONCLUSIONS

The simulation results have shown that a set of ranging measurements from an aircraft to an array of reflectors, such as would be obtained from a scanning pattern, can provide strong recovery of both baselines and relative reflector heights. Extensive further analysis is, however, needed to determine the optimum parameters for both positioning the reflectors and in processing the data collected.

The experimental results demonstrated laser ranging measurements from an aircraft to ground based reflectors, with recorded hits consistent with that expected on the basis of the number of reflectors covered by laser footprints. However, it is noted that "normal" ground returns can, for certain types of terrain, be as strong as reflector returns. Thus, future tests and operational systems must be able to discriminate against ground returns, on the basis of range gating, pulse shape, or some other scheme. Such discrimination is simplified if the geographical region in which the retros are deployed contains only terrain with low, monotonous reflectivities. Unfortunately, fault boundary regions do not always possess such characteristics.

An additional spin-off result of this project is displayed in Figure 11. The information contained therein shows promise for the utilization of an airborne laser system in other remote sensing data collection activities, such as land use.

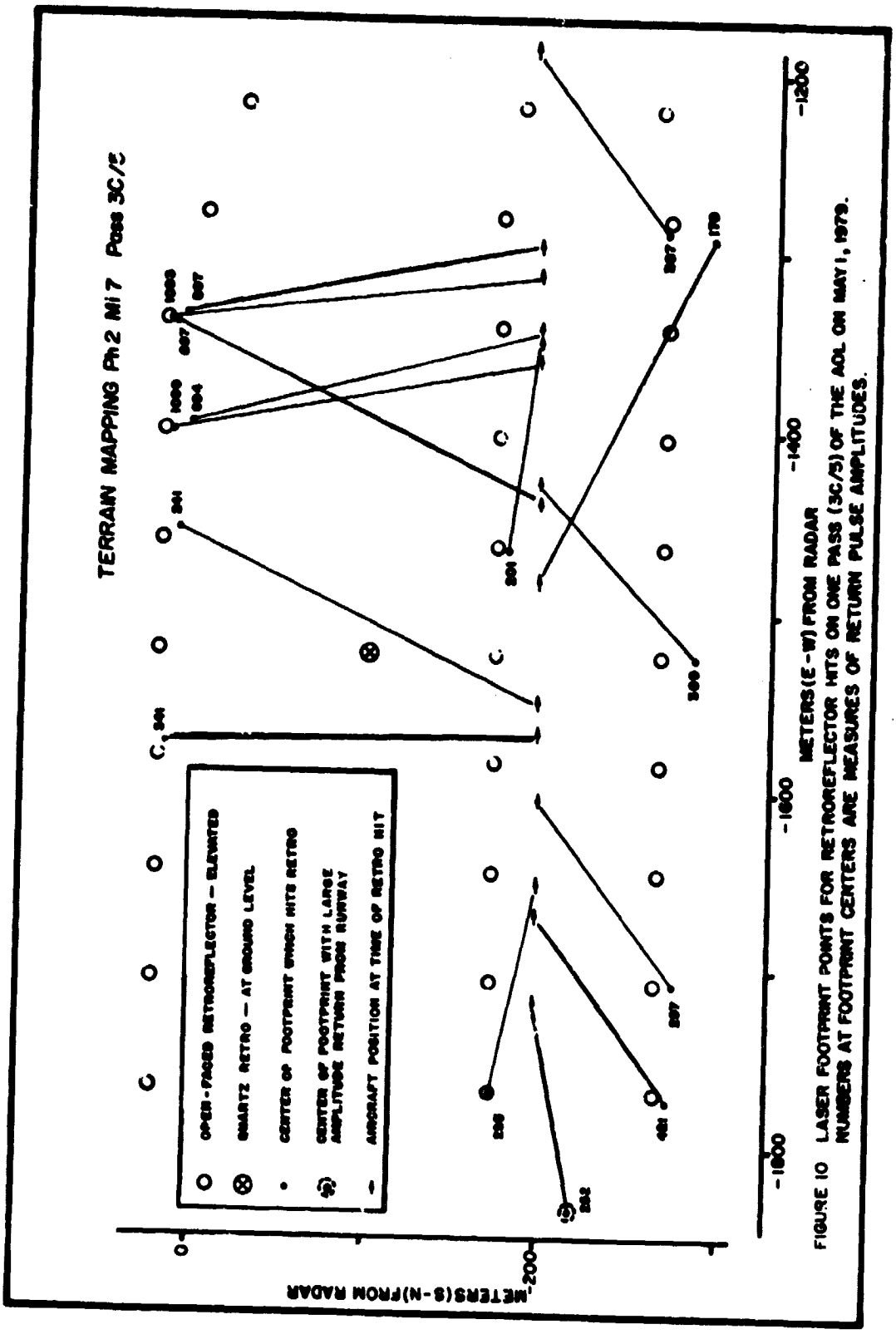

FIGURE 10 LASER FOOTPRINT POINTS FOR RETROREFLECTOR HITS ON ONE PASS (3C/3) OF THE AOL ON MAY 1, 1979. NUMBERS AT FOOTPRINT CENTERS ARE MEASURES OF RETURN PULSE AMPLITUDES.

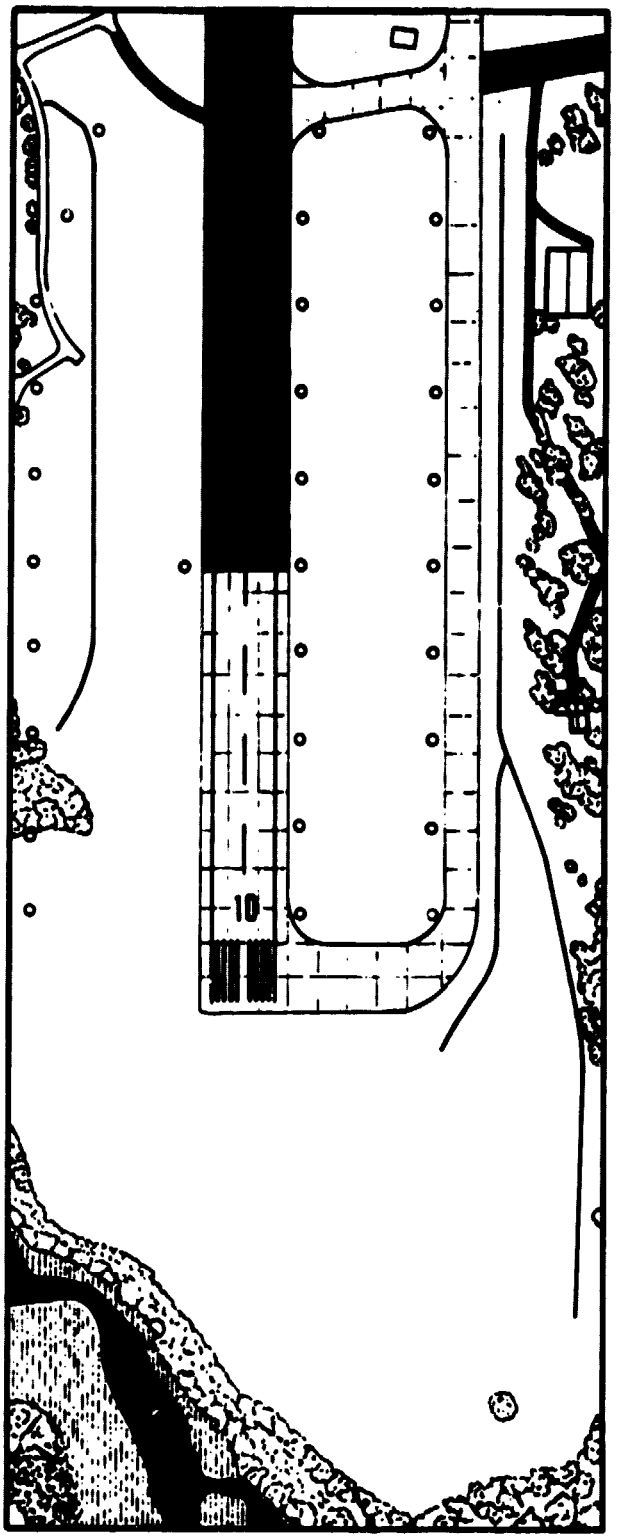

FIGURE 11 RUNWAY GEOMETRY SHOWING DEPLOYED RETROS (CIRCLES) AND ADJACENT TERRAIN

FIGURE 12 CONTOUR MAP OF SURFACE RETURN INTENSITY FROM RUNWAY AREA WITH DEPLOYED RETRO-REFLECTORS. DOTTED CONTOURS SURROUND REGIONS OF MAXIMUM RETURN INTENSITY.

REFERENCES

1. Smith, David E., "Spaceborne Ranging System," Proceedings of the 9th GEOP Conference, An International Symposium on the Applications of Geodesy to Geodynamics, Oct. 2-5, 1978. Dept. of Geodetic Science Report No. 280, The Ohio State University, Columbus, Ohio, pp. 59-64.
2. Kaula, W. M., "Geodynamic Problems," Proceedings of the 9th GEOP Conference, An International Symposium on the Applications of Geodesy to Geodynamics, October 2-5, 1978. Dept. of Geodetic Science Report No. 280, The Ohio State University, Columbus, Ohio, pp. 345-351.
3. Kumar, M., and I. I. Mueller, "Detection of Crustal Motion Using Spaceborne Laser Ranging Systems," Bull. Geod. 52, pp. 115-130, 1978.
4. Kahn, W. D., F. O. Vonbun, D. E. Smith, T. S. Englar, and B. P. Gibbs, "Performance Analysis of the Spaceborne Laser Ranging System," NASA TM 80330, October 1979.
5. Kumar, M., "Monitoring of Crustal Movements in the San Andreas Fault Zone by a Satellite-Borne Ranging System," Dept. of Geodetic Science Report No. 243, The Ohio State University, Columbus, Ohio, August 1976.
6. Smith, D. E., and B. D. Tapley, "The Report from the Workshop on The Spaceborne Geodynamics Ranging System," IASOM TR 79-2 Institute for Advanced Study in Orbital Mechanics, The University of Texas at Austin, Texas, March 1979.
7. Vonbun, F. O., W. D. Kahn, P. D. Argentiero, and D. W. Koch, "Spacebone Earth Applications Ranging System (SPEAR)," Jr. Spacecraft and Rockets 14, pp. 492-495, 1977.
8. Martin C. F., "Partitioned Solution for a Sequential Estimator Using Multiple Data Sets," EG&G Washington Analytical Services Center Report No. PSD 006-79, prepared for NASA Wallops Flight Center under Contract No. NAS6-2823, August 28, 1979.
9. Pavlis, E. C., "Error Analysis for a Spaceborne Laser Ranging System," Dept. of Geodetic Science Report No. 290, The Ohio State University, Columbus, Ohio, December 1979.
10. Aldrich, G. T., "Final Technical Report for Kalman Program for Positioning Aircraft (KAPPA)," Wolf Research and Development Corporation Report PSD 004-71, prepared for NASA Wallops Flight Center under Contract No. NAS6-1942, October 1971.
11. AVCO Everett Research Laboratory, Airborne Oceanographic Lidar System, Final Report, NASA Contractor Report CR-141407, Contract NAS6-2653, October 1975.
12. Martin T. V., W. F. Eddy, A. Brenner, B. J. Rosen, and J. McCarthy, "GEODYN System Description," I, EG&G Washington Analytical Services Center, Riverdale, MD, Feb. 1980.
13. Smithsonian Astrophysical Observatory Staff, "Study of a Close-Grid Geodynamic Measurement System," SAO Reports in Geoastronomy No. 5, 1977.